Heliyon 7 (2021) e06946

Contents lists available at ScienceDirect

Heliyon

journal homepage: www.cell.com/heliyon

Research article

Specifying of aquifer characteristics using forward and inverse modeling of DC-resistivity and TEM methods

A.I. Ammar [a,*], A.S.A. Abu El-Ata [b], A.A. Mustafa [a], A.M.S. Lala [b]

[a] Research Institute for Groundwater, National Water Research Center, Egypt
[b] Geophysics Department, Faculty of Science, Ain-Shams University, Egypt

ARTICLE INFO

Keywords:
DC-Resistivity method
TEM Method
Forward model
Inverse model
Ramp-off time effect
Faults determination
Well logging analysis
Aquifer characterization

ABSTRACT

Exploration and determination of the hydro-geo-electrical characteristics of an aquifer can be done by applying the forward (initial multi-layers), and the inverse (final layered) models for interpreting the DC-resistivity (VES) and TEM data. So, 22 VES using Schlumberger configuration (AB/2 = 500–700m) and 12 TEMS using in-loop configuration (square, ℓ = 200m) were carried out at the West El-Minia selected area for studying the Oligocene Clastic and Carbonate aquifers. VESs were interpreted for studying the shallow resistive and conductive layers, as well as faults delineation. TEMs were interpreted for shallow and deep conductive layers discrimination. The VES and TEM inverse models were examined with the drilling data and construed the subsurface into four units; dry Oligocene Clastics (173–467 Ω.m), dry limestone (273–374 Ω.m), saturated Oligocene Clastics (Oligocene aquifer) (2–107 Ω.m), then saturated fractured Eocene limestone to shaly limestone (5–188 Ω.m). Groundwater depths (62–131m) and thicknesses variation were estimated, as well as the faults location. Two hydro-geo-electrical sections were built for simulating the resistivity values and their connotations, and managing in choosing the promised locations for drilling wells. The ramp-off time effect was studied and found that ~50–~100m shallow high resistive thickness didn't defined from the TEM data in which the max penetration depth was 672m. The available well logging data were analysed to reveal the pure saturated zones, the volume of shale of 0%–100% and the porosity values of ~9%–~35% in the Oligocene aquifer and of ~4%–~15.5% in the carbonate aquifer. So, the forward and inverse models application and soundings integration are considered robust tools for estimating and simulating the aquifer characteristics.

1. Introduction

Generally, the electrical resistivity method like DC-resistivity method (VES) and electromagnetic method like time-domain or transient electromagnetic method (TDEM or TEM) are the common applied methods for near-surface and deep subsurface exploration and in groundwater investigations, because of the good correlation between electrical characteristics of the rocks and their fluid content (Flathe, 1955; Zohdy, 1969; Fitterman and Stewart, 1986; McNeill, 1990; Christensen and Sørensen, 1995; Massoud et al., 2009; and Khalil et al., 2013). TEM soundings have been used extensively for exploring and mapping the changes in groundwater aquifers and their quality depending on their conductivity variation (Stewart and Gay, 1986; Kruse et al., 1998). Also, TEM method has been used in hydrogeological investigation, because of its ability and accuracy in differentiating between the resistivities of formations (Goldman and Neubauer, 1994). Nabighian and Macnae (1991) reported that TEM soundings are good in delineating layered structures of interest, as well as exploration of groundwater aquifers. Both DC-resistivity and TEM methods are widely used in many geophysics applications, including hydrogeological studies as stated by Goldman et al. (1994); Albouy et al. (2001); Danielsen et al. (2003); Jens et al. (2003); Jorgensen et al. (2003); Carrasquila and Ulugergerli (2006).

In general, groundwater is one of the interesting water resources for different life uses, especially at the arid and semi-arid regions. Egypt draws a considerable attention for developing the Western Desert, due to the natural growth of agricultural, industrial and civil activities. So, the hydro-scientists got their attentions to explore the groundwater aquifers in this arid region. The present work aims to study the aquifer characteristics, with focusing on the hydrogeological and geological settings, using the forward and inverse modeling in interpreting the geophysical measurements in West El-Minia area, which located between latitudes 28° 00′ 00″and 28° 30′ 00″ N and longitudes 30° 05′ 0″and 30° 30′ 00″ E

* Corresponding author.
E-mail addresses: abdallah_ammar@nwrc.gov.eg, abdallah_ammar_708@hotmail.com (A.I. Ammar).

https://doi.org/10.1016/j.heliyon.2021.e06946
Received 6 May 2020; Received in revised form 21 June 2020; Accepted 26 April 2021

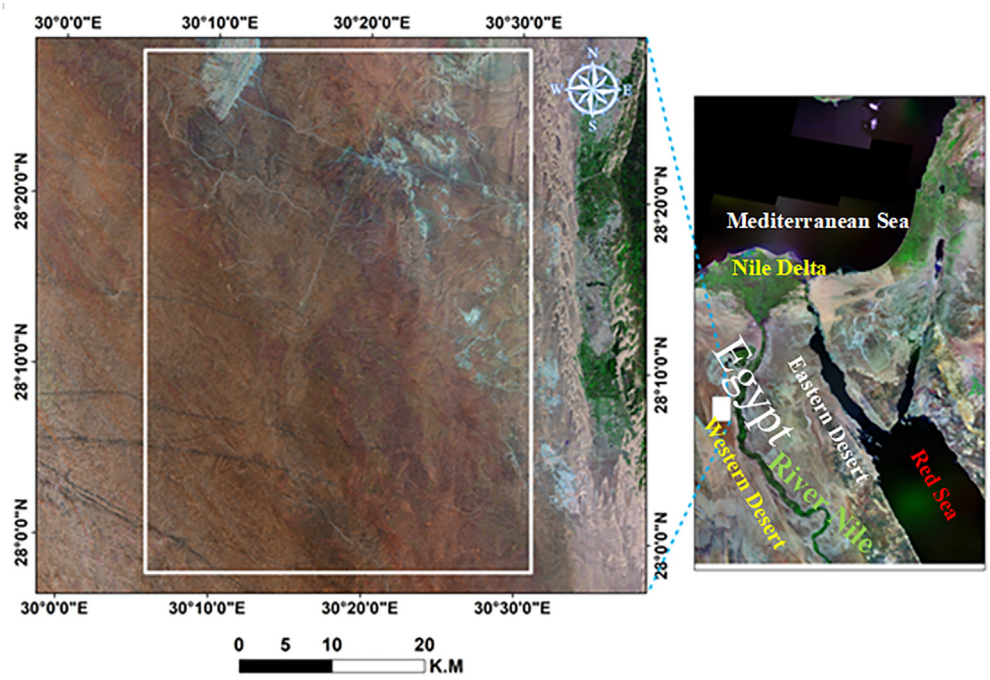

Figure 1. Satellite imaging for showing the general location map of the study area (right panel) and the main boundaries of the study area (left panel).

(Figure 1, left panel). It is located approximately 228km south of Cairo city, on the western side of the River Nile (Figure 1, right panel).

Accordingly, for achieving the previous goals, the DC-resistivity and TEM methods were used to define the aquifer characteristics of holding sediments, such as differentiating the electrical, geological, and hydro-geological characteristics between aquifers (the Eocene fractured limestone and the Oligocene Clastics), the distribution of shale or clay content at these aquifers, estimating and mapping the groundwater levels or depths, and the thickness variations of these aquifers, delineating the structural faults for understanding the hydro-geologic and geologic settings of the groundwater aquifers, as well as the groundwater quality estimation. Also, there are several well logging recordings at this study were used to support the previous DC-resistivity and TEM methods in determining the pure saturated zones and calculating the shale volume and porosity ranges of the saturated layers.

1.1. Geomorphology

Several authors described the geology and geomorphology of West-El-Minia area (Said, 1981; Khalifa, 1981; and Klitszch et al., 1987). In general, the low plains and elevated structural plateaus are the two main geomorphological regions in Egypt. The Nile valley extent between the western slightly drained Eocene plateaus, which include the selected study area, and the eastern highly drained. Where there are several wadies dissect the plateau into elongated northwest or southwest trend (El sayed, 2016). So, along the selected study area, the following features can be recognized (Said, 1981) are young alluvial plains and old alluvial plains of the Nile valley, fanglomerates, calcareous structural plateaus, sand dunes (Figure 4, B), and hydrographic pattern.

At this study, the digital elevation model (DEM) was used to clarify the features along the study area. Figure 2 shows these features to explore and define the gradual change in the topographic elevation from west to east and from south to north. Accordingly, the elevations along the study are ranged from ~202m, in the northwest, to less than ~70m, in the east and north east.

1.2. Surface geology

El-Minia's geological surface is composed of a group of formations ranged from Tertiary era (Early Eocene) until Quaternary era (Holocene).

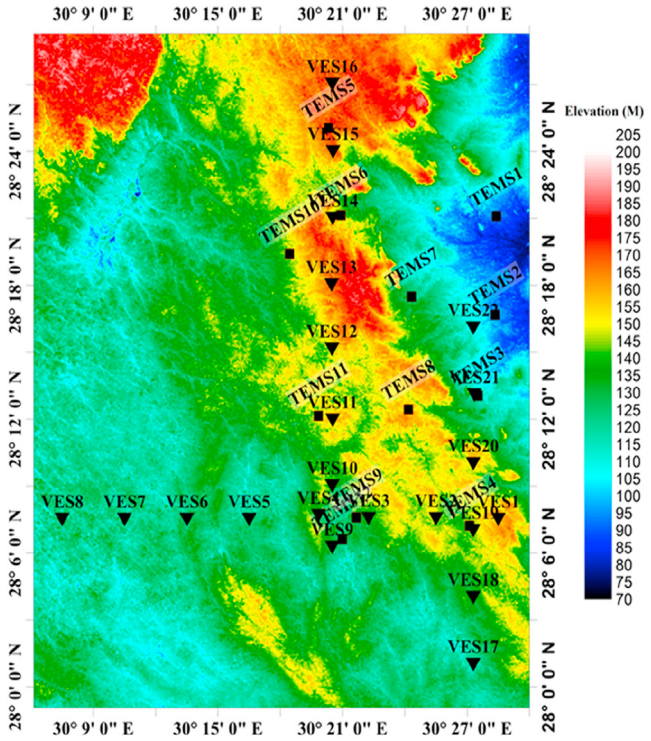

Figure 2. The study area digital elevation model, with the distribution of the measured VES and TEM soundings.

The exposed surface rock units vary from top to base as: Nile silt in the alluvial plain, narrow strips of Pleistocene sands, Oligocene volcanic extrusive rocks, Qatrani Formation sandstones and Eocene limestone, which exposed to the west and east of the River Nile, due to the extensive faulting and uplifting (Khalifa, 1981).

The exposed rock units, as shown on Figure 3, contain the following: Gabal Qatrani Formation, Wadi El-Rayan Formation (limestone intercalated with shale and sandy shale), Oligocene basaltic intrusion (dykes) (Figure 4A), wadi-deposits, El-Minia Formation (limestone), prenile

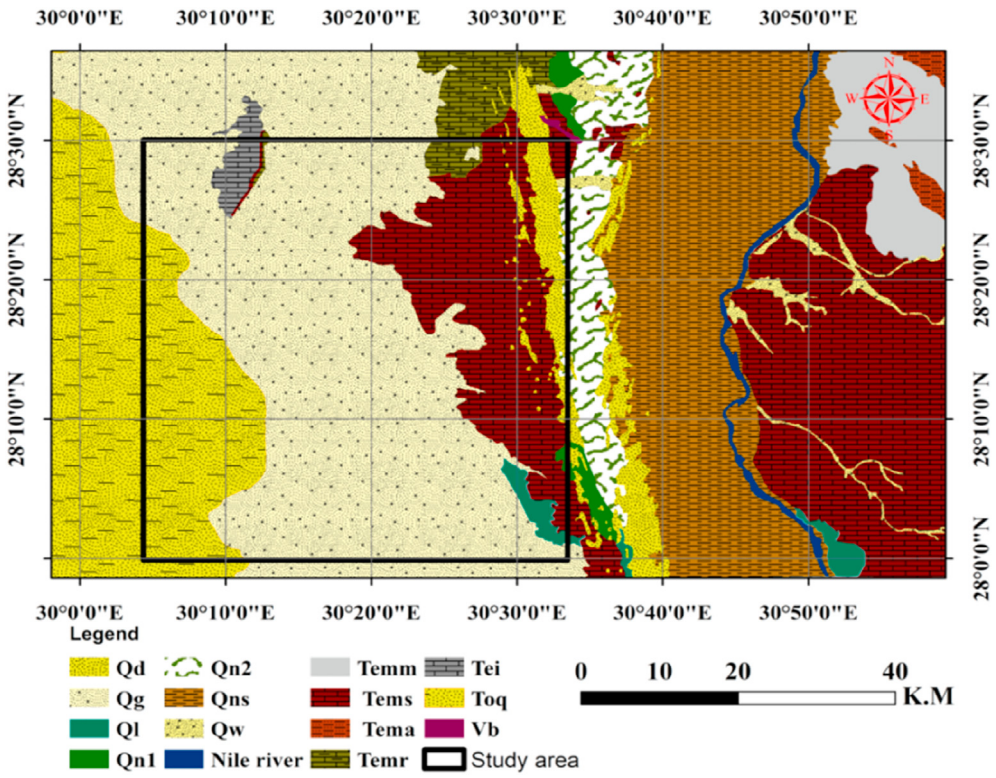

Figure 3. General surface geologic map includes the study area (reprinted and modified after Klitszch et al., 1987). Where Qg: gravel, Ql: fanglomerate, Toq: Gabal Qatrani Formation (sandstone), Temr: Wadi El-Rayan Formation (limestone intercalated with shale and sand shale), Qn1: Protonile deposits, Vb: Oligocene Basaltic dykes, Qw: Wadi-deposits, Tei: El-Minia Formation (limestone), Qn2: Prenile deposits, Qd: sand dunes, Tema: Qarara Formation (shale to siltstone), Qns: Nile silt, Temm: Maghagha Formation (limestone to marl), and Tems: Samalut Formation (Nummulitic limestone).

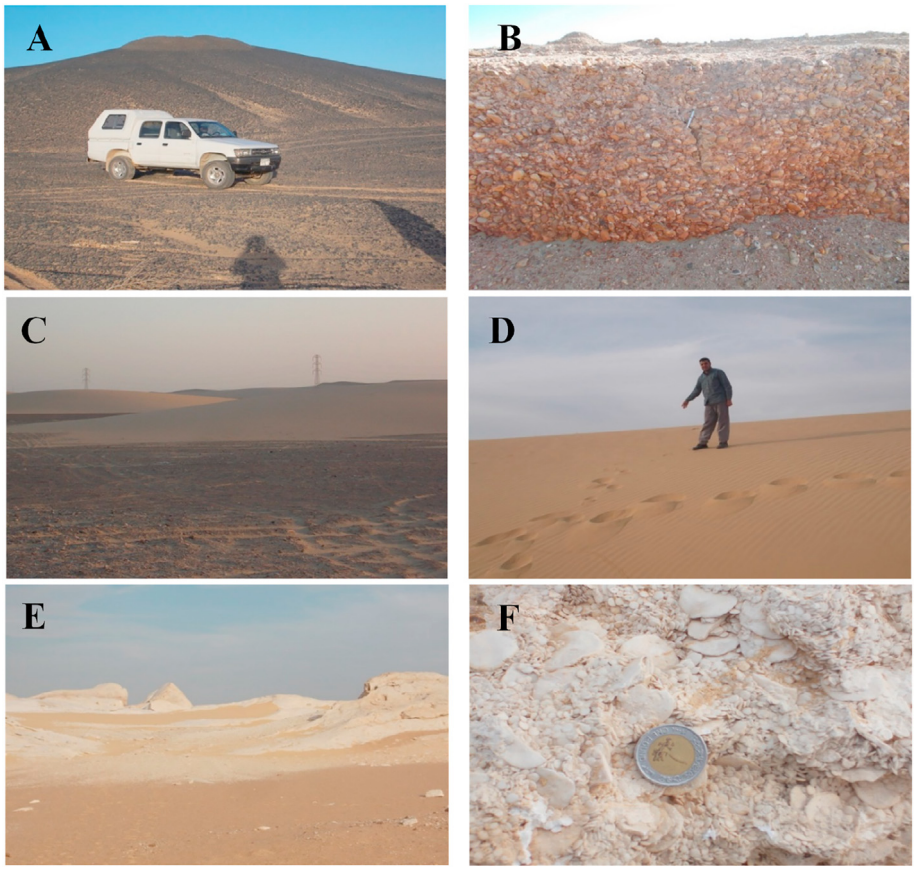

Figure 4. Field photographs for the Oligocene basaltic intrusion (A), outcrop of the Oligocene Clastics (B), sand dunes (C and D), and Nummulitic limestone (Samalut Formation) (E and F).

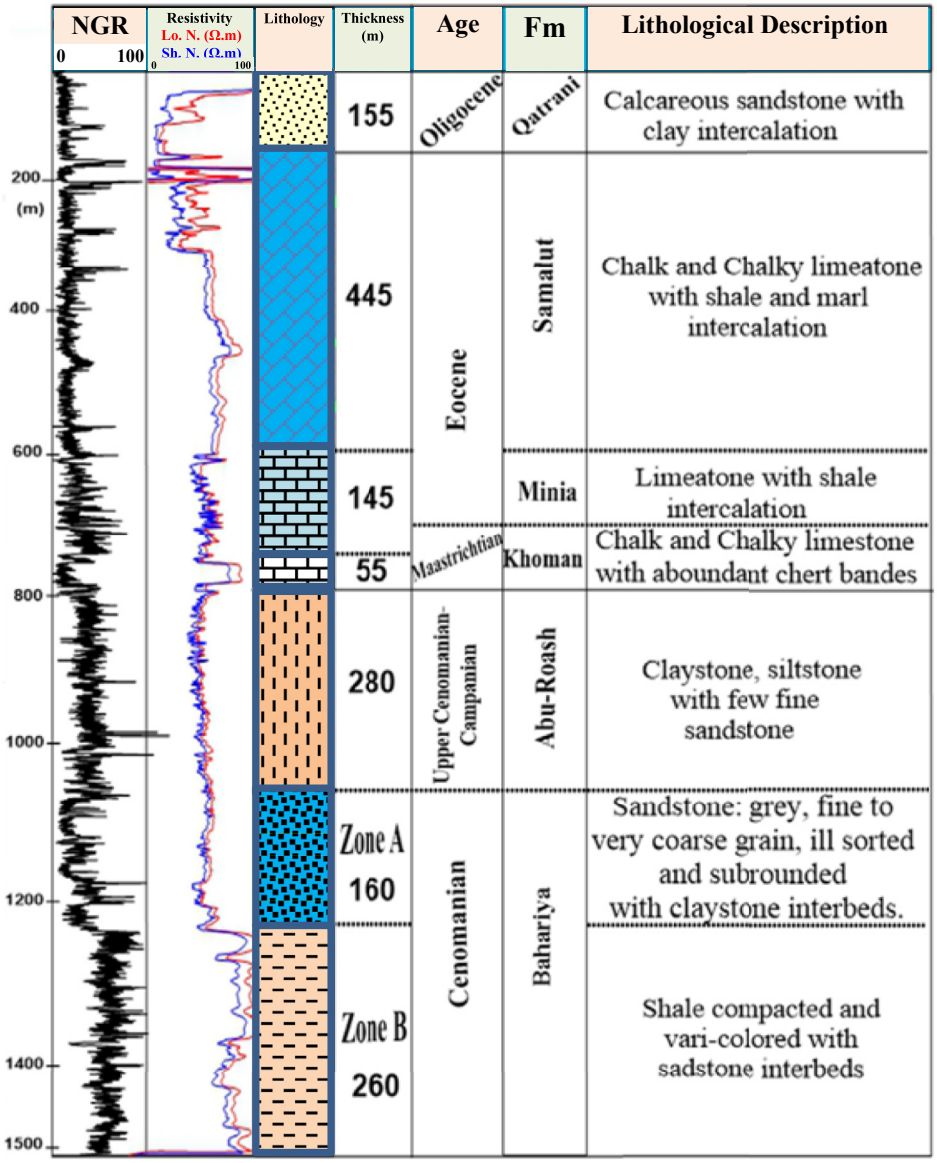

Figure 5. Local litho-stratigraphic column, with composite log located 28^{O} 25$^{\backslash}$ 48$^{\backslash\backslash}$ N and 29^{O} 54$^{\backslash}$ 6.6$^{\backslash\backslash}$ E (reprinted and modified after Yousif et al., 2018).

deposits, sand dunes (Figure 4, C and D), Qarara Formation (shale to siltstone), Nile silt, Maghagha Formation (limestone to marl), Samalut Formation (Nummulitic limestone) (Figure 4, E and F), as well as the outcrop of Oligocene Clastics (Figure 4B).

1.3. Litho-stratigraphy

The local litho-stratigraphic sequence is ranged from Lower Eocene to Recent, as shown on Figure 5 (reprinted and modified after Yousif et al., 2018) and represented by several formations. Bahariya Formation is exposed at the Bahariya Oasis and consists of friable variegated sands, sandstones and claystone, with hard brown ferruginous bands (Said, 1962). Abu Roash Formation is composed of limestone succession, with interbeds of shale and sandstone (Norton, 1967; and Hantar, 1990). Khoman Formation consists of white chalk and chalky limestone with abundant chert (Issawi et al., 1999). El-Minia Formation is made up of snow white limestone (Khalifa, 1981). Samalut Formation is made up of limestone with Nummulite gizehensis (Figure 4, E and F) (Khalifa, 1981). Qatrani Formation (Oligocene) consists of sandstones and quartzite (Khalifa, 1981).

1.4. Structural geology and tectonics

The geologic structures, especially the faults, played an important role in configuring the Eocene limestone plateau add to its effect on the groundwater movement into the carbonate aquifer and between the deep sandstone aquifer. Generally, the structural setting of the north Western Desert is represented by positive and negative undulations, which took place during the Eocene and Oligocene times. The undulations trends in the NNW-SSE direction are assumed to be associated with the NW-SE fault system dominant in the north of Egypt. Other structural features as the elongated folds plunging NW and connected with the NW-SE fault system. This simple structural configuration is further complicated by another trend of folds having a NE-SW, according to Shata (1953) and Said (1962).

Also, Khalifa (1981) reported that, West El-Minia area is characterized by relatively complicated structural settings, which were previously believed to be due to compressive stresses, developing both faulting and folding. Faults are predominating structural elements at this area and are mostly observed at the NW-SE direction (Gulf of Suez Trend) and some follow NNE-SSW direction (Syrian Arc Trend) and they are normal faults.

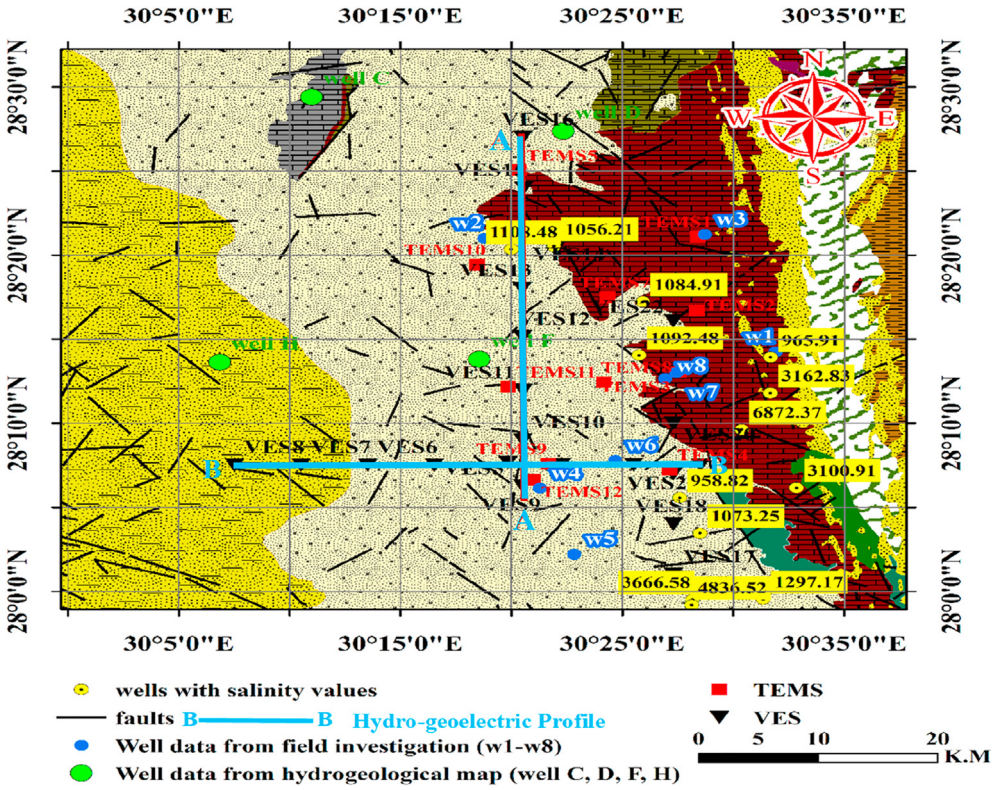

Figure 6. Structural geological map (reprinted and modified after Klitszch et al., 1987) with the sites of all data projected (VESs, TEMs, Shallow wells, and deep wells), as well as the wells with calculated salinity in ppm and hydro-geo-electric sections (A-A and B-B).

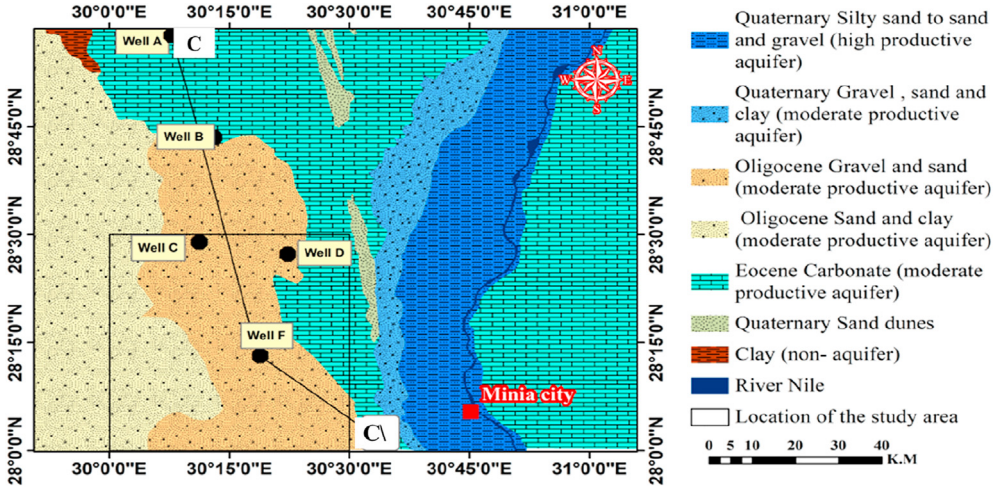

Figure 7. General hydro-geological map of west El-Minia area include the study area [square shape] and the main aquifers (reprinted and modified after RIGW, 2015).

There were some structural features related-faulting, such as grabens and horsts. The distribution of faults along the study area was shown on Figure 6, as delineated from geological map (Klitszch et al., 1987).

1.5. Local hydrogeology

The area under consideration includes a group of aquifers, as reported on the general hydrogeological map (Figure 7). The main two aquifers under study are:

1 Oligocene sand and gravel aquifer system:

This aquifer is composed of gravel and sand with clay intercalations, and its productivity is moderate (RIGW, 1990) and mainly depending on the clay content. If the clay content is high, the productivity will be low and vice versa.

2 Eocene Carbonate aquifer system:

This aquifer is composed mainly of fractured limestone to shaly limestone and its productivity, in general, is moderate and depending on the shale content and fracture density.

Generally, the fractured carbonate aquifer appears to the east and west of the River Nile and considered as important aquifer at the selected area for study, as well as the Oligocene aquifer. RIGW (1990) reported that, the groundwater in the carbonate aquifer had upwarded from the underlying Nubian Sandstone aquifer due to the hydraulic connection between two aquifers, through the vertical major fractures (faults), and

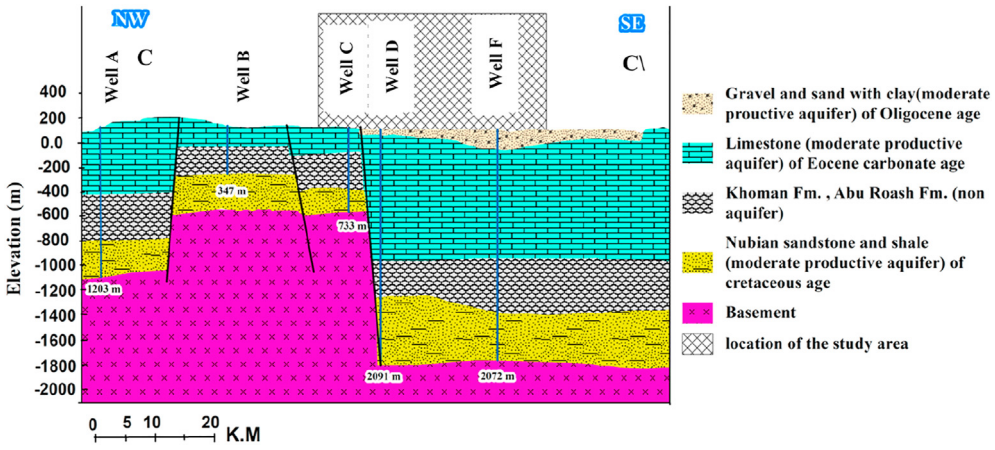

Figure 8. General hydrogeological section C-C\ from NW-SE passing through the study area (reprinted and modified after RIGW, 2015).

Table 1. Coordinates, total depth, depth to groundwater and the aquifer type of the collected drilled wells (8) along the study area, as well as W1 and W5 include well logging data.

Well no.	N	E	Total Depth (m)	Depth to groundwater (m)	Aquifer type
W1	28° 14′ 14″	30° 31′ 54″	204	56	Eocene Carbonate
W2	28° 21′ 00″	30° 18′ 46″	180	115	Eocene Carbonate
W3	28° 21′ 13″	30° 28′ 43″	160	60	Eocene Carbonate
W4	28° 06′ 7.92″	30° 21′ 16″	160	85	Oligocene clastic
W5	28° 02′ 12.4″	30° 22′ 49″	206	90	Oligocene clastic
W6	28° 07′ 47.2″	30° 24′ 40″	200	106	Oligocene clastic
W7	28° 13′ 0.8″	30° 27′ 26″	238	90	Eocene Carbonate
W8	28° 12′ 39″	30° 26′ 55″	238	56	Eocene Carbonate

the formation pressure of the deep aquifer. Figure 8 shows a general hydrogeological section C-C\ passes through the study area, square shape at Figure 7, describes the subsurface hydrogeological units, with focusing on the Oligocene and Eocene carbonate aquifers.

1.6. Well data description

The collected shallow wells (8 wells), as reported in Table 1 and wells (15), with the salinity values, as distributed in Figure 6, were drilled at the Carbonate and Oligocene aquifers. The max depths of the 8 wells are ranged from 160m to 240m. The hydrogeological collected data of these wells include the locations, the total drilling depths and the depths to groundwater (Table 1), as well as the aquifer type. Also, there are four (3) deep productive wells (wells C, D, and F), as distributed on the map (Figure 6). The last four deep wells penetrate the Oligocene, Carbonate and Nubian sandstone aquifers, as shown on the hydrogeological section (Figure 8). Also, this section presents the expected max and min. thicknesses of the previous aquifers along the study area.

2. Materials and methods

2.1. DC-resistivity method

At this method, the direct electric current (DC) method was used for measuring the resistivity of the shallow subsurface resistive and conductive geological layers, with focusing on the shallow resistive

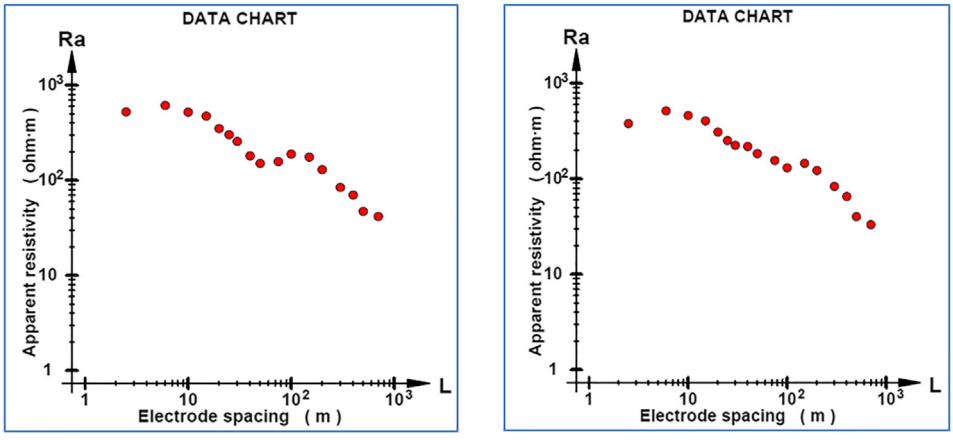

Figure 9. Apparent resistivity curves for sounding VES1 (left) and for sounding VES14 (right).

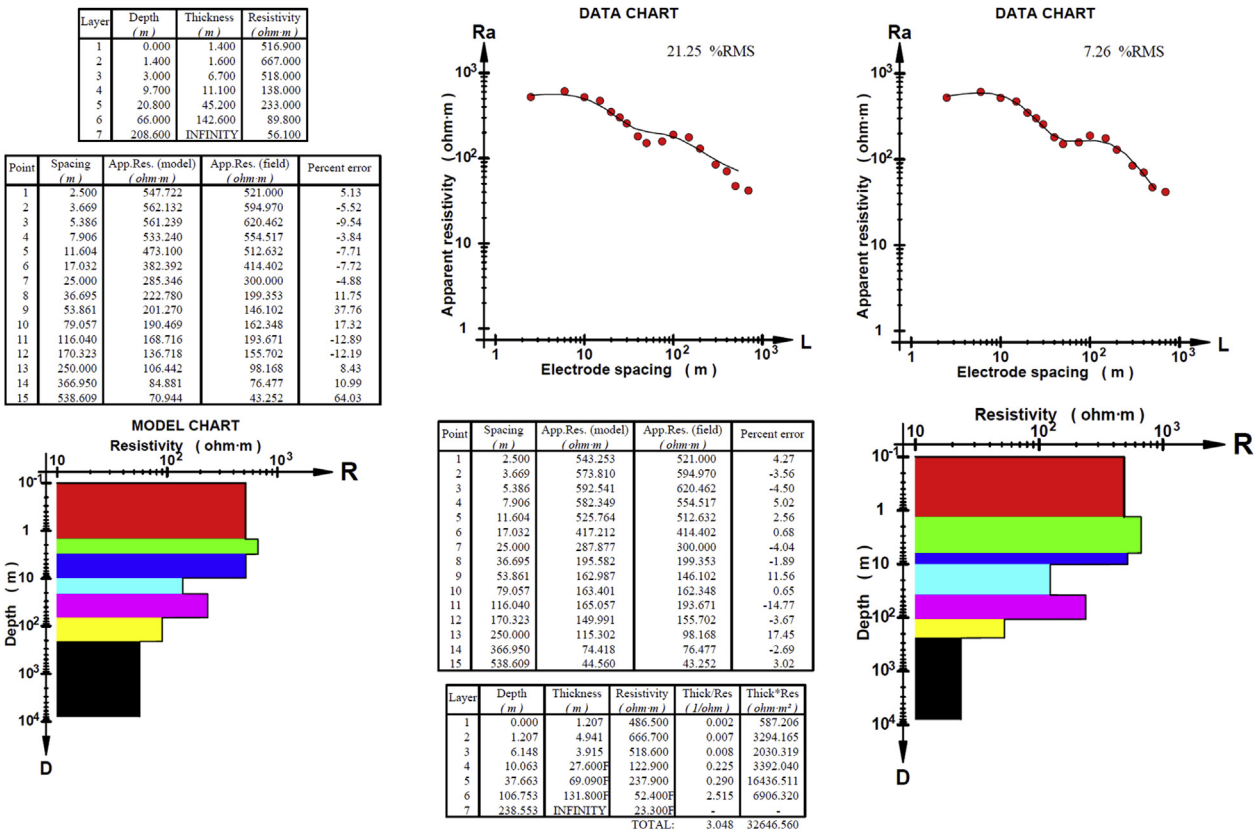

Layer	Depth (m)	Thickness (m)	Resistivity (ohm·m)
1	0.000	1.400	516.900
2	1.400	1.600	667.000
3	3.000	6.700	518.000
4	9.700	11.100	138.000
5	20.800	45.200	233.000
6	66.000	142.600	89.800
7	208.600	INFINITY	56.100

Point	Spacing (m)	App.Res. (model) (ohm·m)	App.Res. (field) (ohm·m)	Percent error
1	2.500	547.722	521.000	5.13
2	3.669	562.132	594.970	-5.52
3	5.386	561.239	620.462	-9.54
4	7.906	533.240	554.517	-3.84
5	11.604	473.100	512.632	-7.71
6	17.032	382.392	414.402	-7.72
7	25.000	285.346	300.000	-4.88
8	36.695	222.780	199.353	11.75
9	53.861	201.270	146.102	37.76
10	79.057	190.469	162.348	17.32
11	116.040	168.716	193.671	-12.89
12	170.323	136.718	155.702	-12.19
13	250.000	106.442	98.168	8.43
14	366.950	84.881	76.477	10.99
15	538.609	70.944	43.252	64.03

Point	Spacing (m)	App.Res. (model) (ohm·m)	App.Res. (field) (ohm·m)	Percent error
1	2.500	543.253	521.000	4.27
2	3.669	573.810	594.970	-3.56
3	5.386	592.541	620.462	-4.50
4	7.906	582.349	554.517	5.02
5	11.604	525.764	512.632	2.56
6	17.032	417.212	414.402	0.68
7	25.000	287.877	300.000	-4.04
8	36.695	195.582	199.353	-1.89
9	53.861	162.987	146.102	11.56
10	79.057	163.401	162.348	0.65
11	116.040	165.057	193.671	-14.77
12	170.323	149.991	155.702	-3.67
13	250.000	115.302	98.168	17.45
14	366.950	74.418	76.477	-2.69
15	538.609	44.560	43.252	3.02

Layer	Depth (m)	Thickness (m)	Resistivity (ohm·m)	Thick/Res (1/ohm)	Thick*Res (ohm·m²)
1	0.000	1.207	486.500	0.002	587.206
2	1.207	4.941	666.700	0.007	3294.165
3	6.148	3.915	518.600	0.008	2030.319
4	10.063	27.600F	122.900	0.225	3392.040
5	37.663	69.090F	237.900	0.290	16436.511
6	106.753	131.800F	52.400F	2.515	6906.320
7	238.553	INFINITY	23.300F	-	-
			TOTAL:	3.048	32646.560

Figure 10. Represents the forward modeling for model (VES1 model) in comparison with VES1 data and RMS% (upper: table, model chart, and data chart) while the lower: table, model chart, and data chart represent the inverse modeling for sounding VES1 with RMS%.

depths and the shallow conductive depths of Carbonate and Oligocene aquifers. So, twenty two (22) VES were carried out, using SAS1000 DC resistivity meter and Schlumberger array configuration with max separation between the current electrodes (AB/2) ranged from ~500 to ~700m. The measured VESs were distributed on the map (Figure 6). These VESs with the TEMs were used for building two hydro-geo-electric sections along the study area. Figure 9 shows two examples of the measured VESs at the study area (VES1, left and VES14, right).

2.2. TEM method

Generally, in the TEM survey, a direct current is passed through a large ungrounded loop to energize it and transform into alternating current. The last current generates an electric field then this field generates primary magnetic field. After that, an electromotive force will be induced into the earth. So, after a discrete period of time, the applied current is switched off abruptly and the primary magnetic field will induce eddy currents within the conductor. These eddy currents will develop a secondary magnetic field, which induces an electromotive force (induced voltage) in the receiving coil (magnetic antenna). This voltage is sampled in high resolution ADC. In our case, the receiver sample resolution is 24 bit. These samples represent information of specific subsurface depth. Eq. (1) describes the induced voltage in the receiver coil with time, as described by Flores et al. (2013):

$$V_{late} = \frac{L^2 I A_R}{20}\left(\frac{\mu_0{}^5}{\pi^3 p^3 t^5}\right)^{0.5} \quad (1)$$

Where: V_{late} is the induced voltage in the receiving coil (Volt), L is the transmitter side length (m), I is the current passed in the transmitter coil (Ampere), A_R is the receiving coil area (m^2), p is the apparent resistivity at a given time (Ω.m), t is the time of sampled voltage (s), and μ_0 is the free air permeability $4\pi \times 10^{-7}$ H/m.

The receiver GDP 32^{24}, to sample the signal developed as induced voltage in the receiving coil at a known time, the transmitter Zt-30, and xmt-G controller, to harmonize the signals between the transmitter and receiver, were used for TEM surveying at this study. Therefore, the resulted shallow resistivity data from VESs were integrated with 12 TEM soundings (Figure 6), which carried out, using Zonge equipment GDP 32^{24}, with in-loop array configuration in the form of a square with side length of 200m, to investigate the shallow and deep subsurface conductive layers.

2.3. Data inversion and interpretation

Both the TEM and VES data were interpreted by applying the forward and inverse models rules. DC-resistivity (VES) data inversion and interpretation were carried out by two complementary softwares. Zohdy Techniques (1989) was used to create the initial model in the form of a multi-layers model, which considered as forward model at Rinvert software (1999). Then after several iterations by using *Rinvert software*, the inverse model, which reflects the layered model, will be created. Figures 10 and 11 represent the forward and inverse models of VES1 and VES14, as two examples of the DC-resistivity method. While the TEM data inversion and interpretation were carried out, basically, through two *Zonge engineering programs;* are *Steminv and Tcinv*. *Steminv program* is considered as smooth-model inversion for converting the TEM measurements to sections of resistivity vs depth, to get the forward model (initial model) by grouping the matched resistivity values, then *Tcinv program* was used for inverting the last forward model to final layered model (inverse model). Figures 12 and 13 represent the forward and inverse models of two examples of the TEMs are TEM4 and TEM12, respectively.

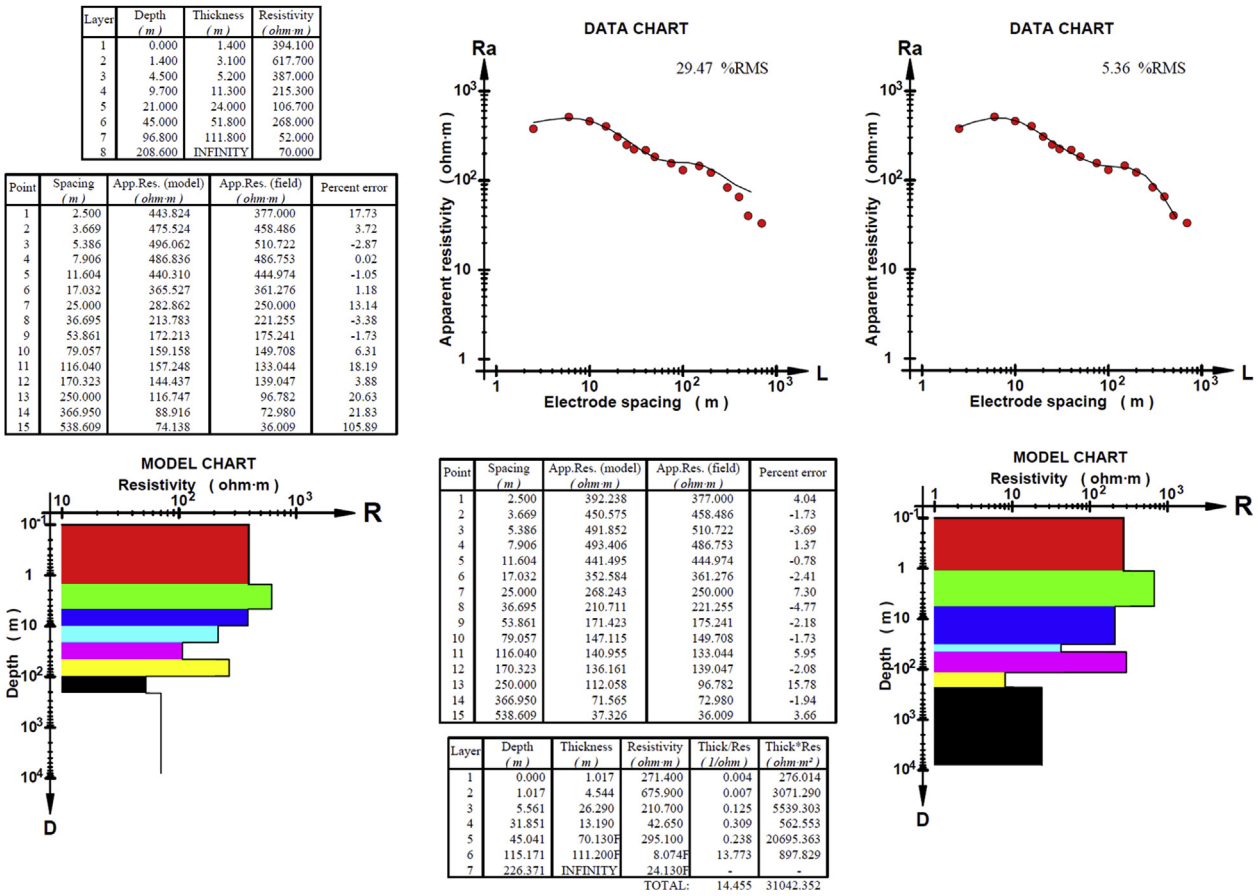

Layer	Depth (m)	Thickness (m)	Resistivity (ohm·m)
1	0.000	1.400	394.100
2	1.400	3.100	617.700
3	4.500	5.200	387.000
4	9.700	11.300	215.300
5	21.000	24.000	106.700
6	45.000	51.800	268.000
7	96.800	111.800	52.000
8	208.600	INFINITY	70.000

Point	Spacing (m)	App.Res. (model) (ohm·m)	App.Res. (field) (ohm·m)	Percent error
1	2.500	443.824	377.000	17.73
2	3.669	475.524	458.486	3.72
3	5.386	496.062	510.722	-2.87
4	7.906	486.836	486.753	0.02
5	11.604	440.310	444.974	-1.05
6	17.032	365.527	361.276	1.18
7	25.000	282.862	250.000	13.14
8	36.695	213.783	221.255	-3.38
9	53.861	172.213	175.241	-1.73
10	79.057	159.158	149.708	6.31
11	116.040	157.248	133.044	18.19
12	170.323	144.437	139.047	3.88
13	250.000	116.747	96.782	20.63
14	366.950	88.916	72.980	21.83
15	538.609	74.138	36.009	105.89

Point	Spacing (m)	App.Res. (model) (ohm·m)	App.Res. (field) (ohm·m)	Percent error
1	2.500	392.238	377.000	4.04
2	3.669	450.575	458.486	-1.73
3	5.386	491.852	510.722	-3.69
4	7.906	493.406	486.753	1.37
5	11.604	441.495	444.974	-0.78
6	17.032	352.584	361.276	-2.41
7	25.000	268.243	250.000	7.30
8	36.695	210.711	221.255	-4.77
9	53.861	171.423	175.241	-2.18
10	79.057	147.115	149.708	-1.73
11	116.040	140.955	133.044	5.95
12	170.323	136.161	139.047	-2.08
13	250.000	112.058	96.782	15.78
14	366.950	71.565	72.980	-1.94
15	538.609	37.326	36.009	3.66

Layer	Depth (m)	Thickness (m)	Resistivity (ohm·m)	Thick/Res (1/ohm)	Thick*Res (ohm·m²)
1	0.000	1.017	271.400	0.004	276.014
2	1.017	4.544	675.900	0.007	3071.290
3	5.561	26.290	210.700	0.125	5539.303
4	31.851	13.190	42.650	0.309	562.553
5	45.041	70.130F	295.100	0.238	20695.363
6	115.171	111.200F	8.074F	13.773	897.829
7	226.371	INFINITY	24.130F	-	-
			TOTAL:	14.455	31042.352

Figure 11. Represents the forward modeling for model (VES14 model) in comparison with VES14 data and RMS% (upper: table, model chart, and data chart) while the lower: table, model chart, and data chart represent the inverse modeling for sounding VES14 with RMS%.

3. Results and discussion

3.1. Ramp-off time effect

The limited accuracy of the TEM method at the shallow depths, especially the resistive depths, is due to the interference between the primary and secondary magnetic fields at the early-stage of the ramp-off time resulted from transmitter, while it is limited at greater depths by the transmitter power and surrounding noises (Stewart and Gay, 1986). So, the shallow resistive thickness ~50m–~100m, as recorded from the VES data, didn't record from the TEM data, due to the effect of ramp-off time. Also, it was deleted during building the hydro-geo-electric sections from the TEM data. In this study, the ramp-off time was 160μs, when the used side length of the loop was 200m.

Therefore, the ramp-off time effect of the data collected from the shallow depths was calculated and described from the diffusion depth Eq. (2) (Spies, 1989; Reynolds, 2011). This for calculating the unrecorded high resistive shallow depths and, also, for calculating the diffusion depth, which indicates the depth of investigation.

$$\delta = \sqrt{\frac{2t\rho}{\mu_o}} = 1.26\sqrt{\rho t} \qquad (2)$$

Where: δ is the depth of investigation at a given time (m), $\mathbf{t}$ is the time (s), ρ is the average high resistivity of the shallower depths (Ω.m) and $\boldsymbol{\mu_o}$ is the free air permeability $4\pi \times 10^{-7}$ H/m.

So, the previous diffusion depth equation has been used to calculate the effect of ramp-off time on the investigated depth, through using different average values of the shallow depths resistivities (ρ) (170 Ω.m, 320 Ω.m and 470 Ω.m), as determined from VES outputs (Figure 14). It appears that, as the ramp-off time increase, the affected depth increase, especially at the shallow resistive depths (Fitterman and Anderson, 1987), as well as the diffusion (investigation) depth increase. The ramp-off time effect becomes large, as the turn-off time increase and the surface resistivity increase. The low resistivities of the shallow depths tend to decrease the effect of ramp-off time pronounced. So, at this study, as resulted from the TEM data inversion and interpretation, the effect of ramp-off time was appeared at the very low resistive values of the shallow thickness (~50–~100m).

3.2. Comparison among the VES inverse models and the TEM inverse models

From the comparison between the VES inverse model and the TEM inverse model, it was found a good matching between the outputs of the two inverse models, especially in case of determining and calculating the level to groundwater and the resistivity values of the aquifers, as reported in Table 2. But, there are exceptions, such as the resistivity of the aquifer at TEM11, that is smaller than the resistivity values at VES11, because of the presence of clay at the top of aquifer, add to the TEM method is more sensitive to the conductive zones, with high content of clay than the DC-resistivity method, and also it is less sensitive to the resistive zones than the DC-resistivity method. Also, the small variation in groundwater level determination from the two methods may be due to the effect of the moisture content at the upper parts of the aquifer.

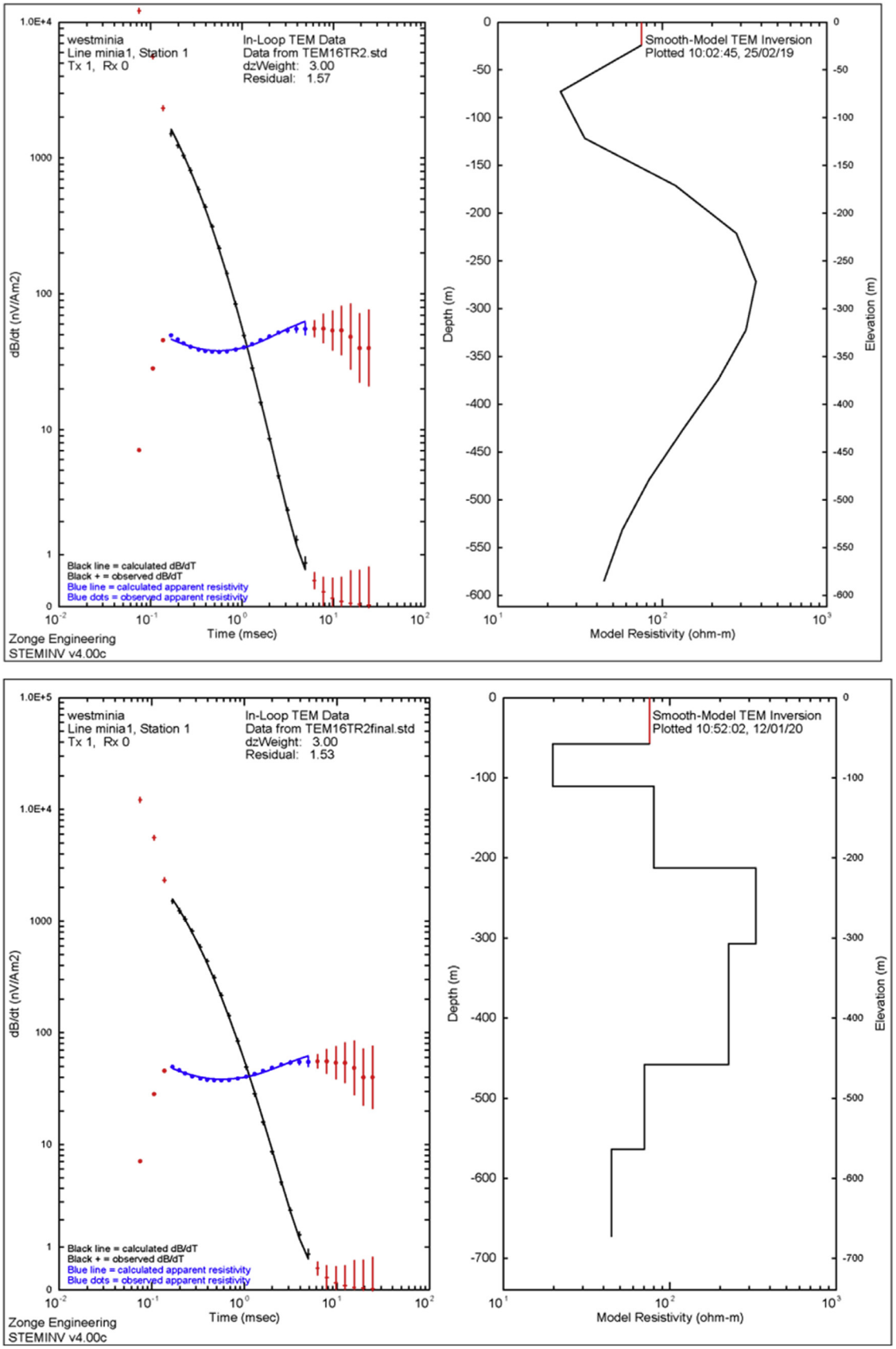

Figure 12. Represents the initial (forward) model for TEM4 which resulted from the initial matching between the measured field data of voltage and resistivity with time (dotted points) and the calculated curves (solid lines) (left) and the final inverse model (earth layered model) of this sounding (right) with residual value.

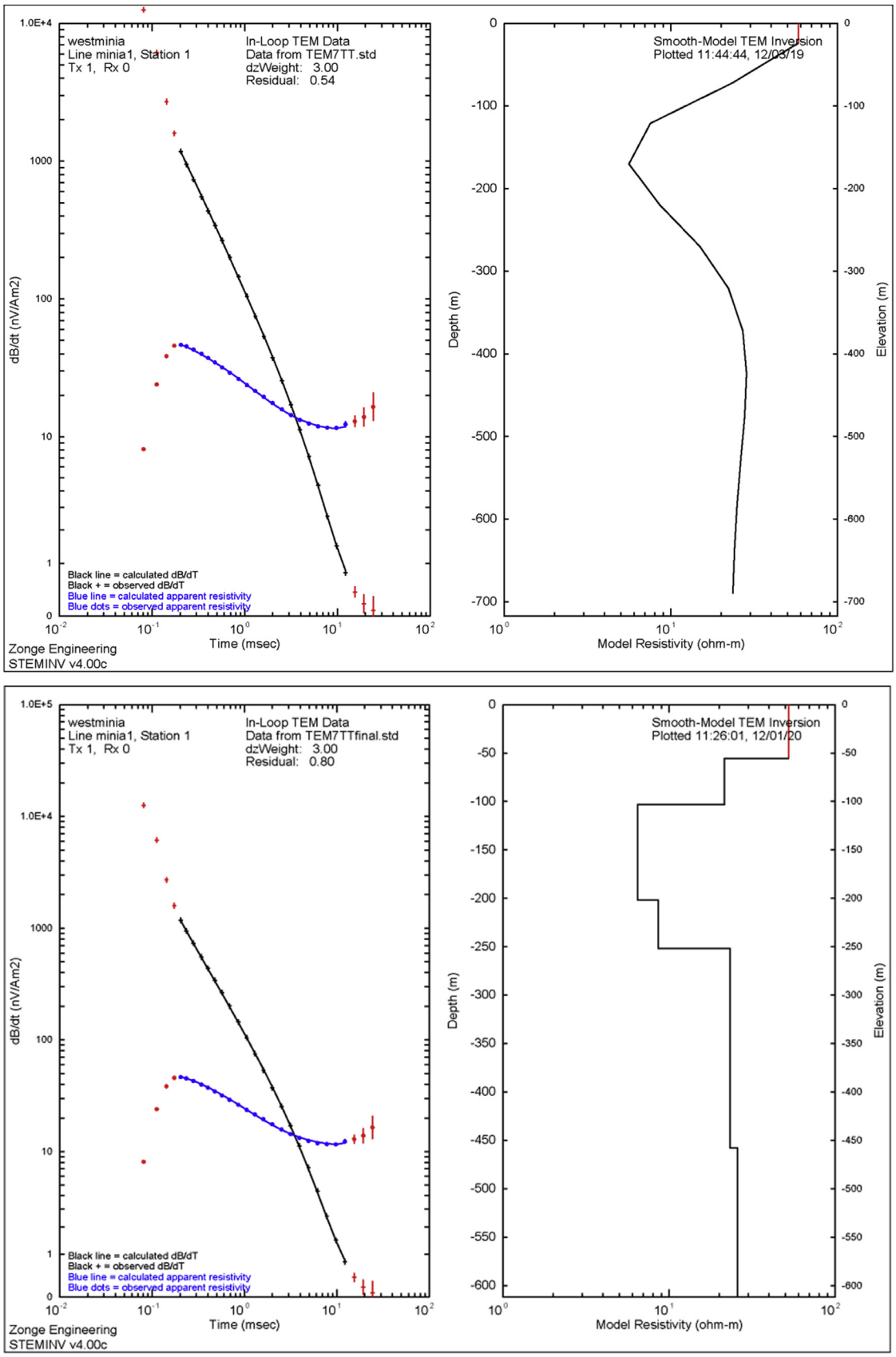

Figure 13. Represents the initial (forward) model for TEM12 which resulted from the initial matching between the measured field data of voltage and resistivity with time (dotted points) and the calculated curves (solid lines) (left) and the final inverse model (earth layered model) of this sounding (right) with residual value.

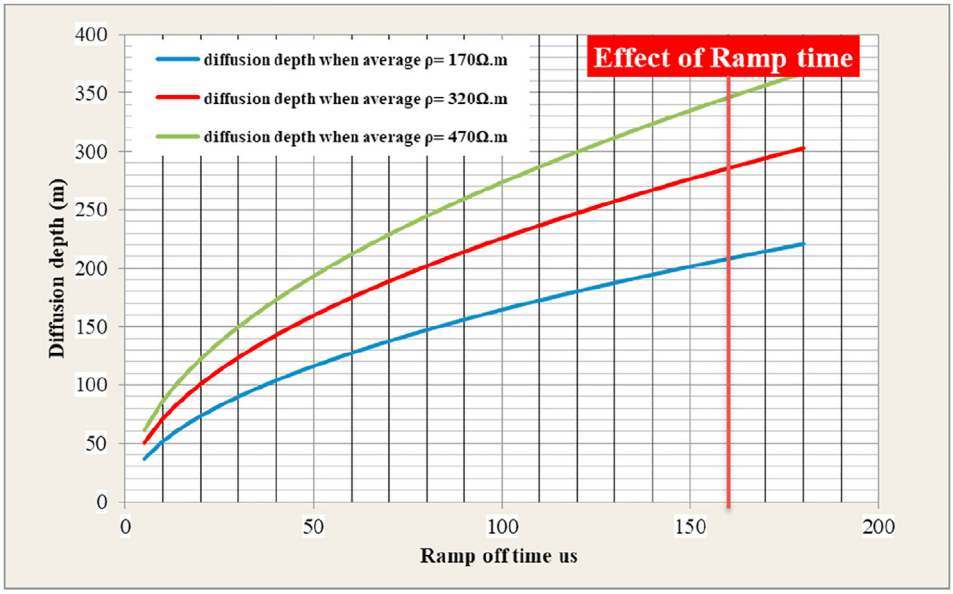

Figure 14. Effect of Ramp-off time on the shallow depths and the investigated depth. Where the olive green line represents the diffusion depth, when the average ρ = 170 Ω.m, the red line represents the diffusion depth, when the average ρ = 320 Ω.m, the dark blue line represents the diffusion depth, when the average ρ = 470 Ω.m.

Table 2. The matching between the DC resistivity and the TEM outputs in determining the groundwater level and resistivity of the aquifer.

Output	TEM 5	VES 15	TEM 6	VES 14	TEM 11	VES 11	TEM 12	VES 9	TEM 4	VES 19	TEM 9	VES 3
Soundings												
Water Level (m)	39	39	57	39.5	60	63	38	31	46.5	47	40	45
ρ (Ω.m)	6	3	10	8	2.2	8	6.5	10	80	62	13	24

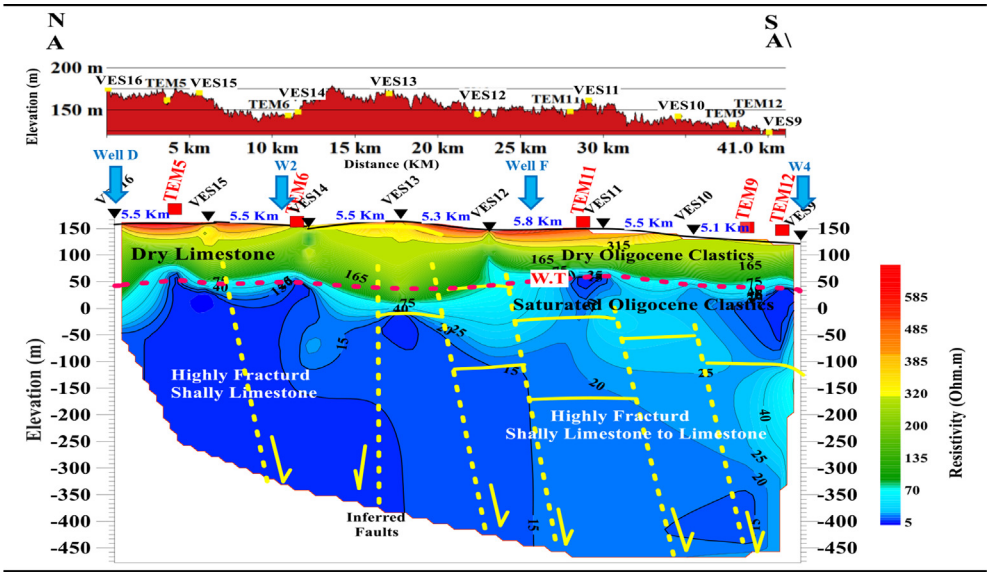

Figure 15. Longitudinal hydro-geo-electrical section AA\, as built from the VESs and the TEMs data inversion and wells data, with the resistivity values distribution and their geological and hydrogeological implications, the lithological distribution and the groundwater levels, as well as determination of the inferred faults.

3.3. Hydro-geoelectrical sections

From the inversion and interpretation of the TEM and VES soundings and carrying out the integration between the two methods, there are several sections were built to show the subsurface geologic layers and the main water-bearing layers along the study area. The longitudinal hydro-geo-electrical section A-A\ (Figure 15) in the N–S direction includes VESs (16, 15, 14, 13, 12, 11, 10, 9), TEMs (5, 6, 11, 9, 12), two deep wells (well D and well F), and two shallow wells (W2 and W4) while the transverse hydro-geo-electrical section B-B\ (Figure 16) in the W-E direction

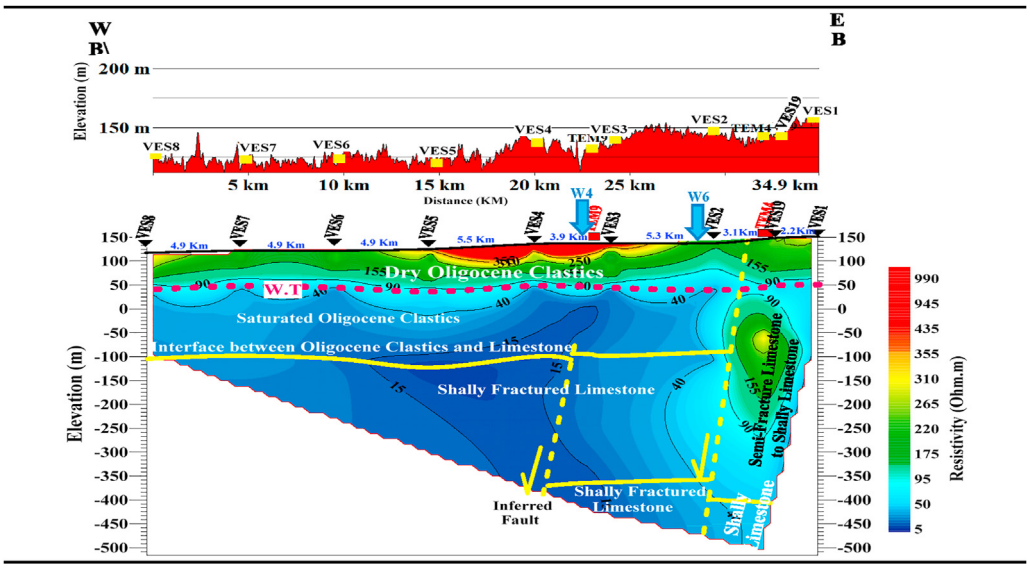

Figure 16. Transverse hydro-geo-electrical section BB\, as built from the VESs and the TEMs data inversion and wells data, with the resistivity values distribution and their geological and hydrogeological implications, the lithological distribution, and the groundwater levels, as well as determination of the inferred faults.

Table 3. Electrical, lithological and hydrogeological characteristics of the recorded geo-electrical units.

Geoelectrical unit	Type of Lithology with hydrogeological Description	Max. ρ (Ω.m)	Min. ρ (Ω.m)	Max. Thickness (m)	Min. Thickness (m)
Unit 1	Dry Oligocene Clastics	(VES11) 467	(VES12) 171	(VES2) 109	(VES7) 78
Unit 2	Dry Eocene Carbonate	(VES22) 374	(VES14) 273	(VES13) 131	(VES22) 68
Unit 3	Saturated Oligocene Clastics	(VES17) 107	(TEM11) 2	(VES18) 169	(VES11) 79
Unit 4	Saturated Eocene Carbonate	(TEM4) 188	(TEM5) 5	(TEM7) 304	(TEM4) 562

includes VESs (8, 7, 6, 5, 4, 3, 2, 19, 1), TEMs (9 and 4), and two shallow wells (W4 and W6). Therefore, these sections were chosen for illustrating the electrical, hydrogeological and geological conditions along the study area.

Generally, the maximum investigated depth from the resistivity method was ~250m and it was ~672m from the TEM method. The resistivity method gave better resolution in the shallow resistive depths than the TEM method. The maximum depth of investigation from the TEMs was deeper than from the VESs. The two sections (Figures 15 and 16) represent four main geo-electric units. These units are the dry Oligocene Clastics and the dry limestone above the groundwater table, especially at the shallow depths, saturated Oligocene Clastics and saturated fractured limestone below the groundwater table at the deep depths. Also, the shale content increases in the limestone aquifer with depth. The electrical properties and their hydrogeological implications, reported in Table 3, are:

- The ***1st*** geo-electric unit is represented by the upper part of the dry Oligocene Clastics layer. This unit is characterized by resistivity values varying from 173 Ω.m - 467 Ω.m, and thickness ranging from 78m - 109m.
- The ***2nd*** unit represents the dry limestone deposits, with variation in resistivity values from 273 Ω.m - 374 Ω.m and in thickness from 68m - 131m.
- The ***3rd*** unit represents the saturated Oligocene Clastics, which is characterized by resistivity values range from 2 Ω.m, due to the increase in clay and salinity, to 107 Ω.m, due to the measurement in sand and gravel and its thickness ranges from 79m - 169m. The variation in thickness is due to the effect of faults.
- While the ***4th*** unit represents the last recorded layer of the saturated Eocene carbonate, which varies in the resistivity values from 5 Ω.m, due to the increase in shale content, salinity and fracture density, to 188 Ω.m, due to the decrease in fracture density and salinity. The maximum penetrated thickness along the study area by the TEM method was 562m, as recorded at TEM4.

Along the previous sections, there are several inferred faults were determined from the matching between the structure map (Figure 6) and the application of the following new assumptions by Ammar and Kamal (2018), which are:

1 There is no fault between the adjacent VESs, if there was coinciding between their resistivity curves.
2 There is fault between the adjacent VESs, if there was intersecting between their resistivity curves. where the intersect point of the two curves is the peak of this fault or the beginning depth to detect the fault criterion, as shown on Figure 17, which represents four examples of the intersection between the resistivity curves of VES11 and VES13, VES12 and VES13, VES18 and VES19, and, also, between VES19 and VES20. In this study, the calculated curves were used instead of the field curves, because the field geo-electric curves were affected by the data noises.

Accordingly and after applying the previous assumptions, it was found good matching of the delineated faults from the structure map and the deduced faults, as shown on Figure (6).

3.4. Well logging analysis

There are two wells (well 1 and well 5) (Table 1) have different types of well logging recordings. Well (1) includes Gamma-ray log, short and long resistivity logs, and calibre log and it was drilled in the limestone aquifer (Figure 18, left), while the well (5), which was drilled in the

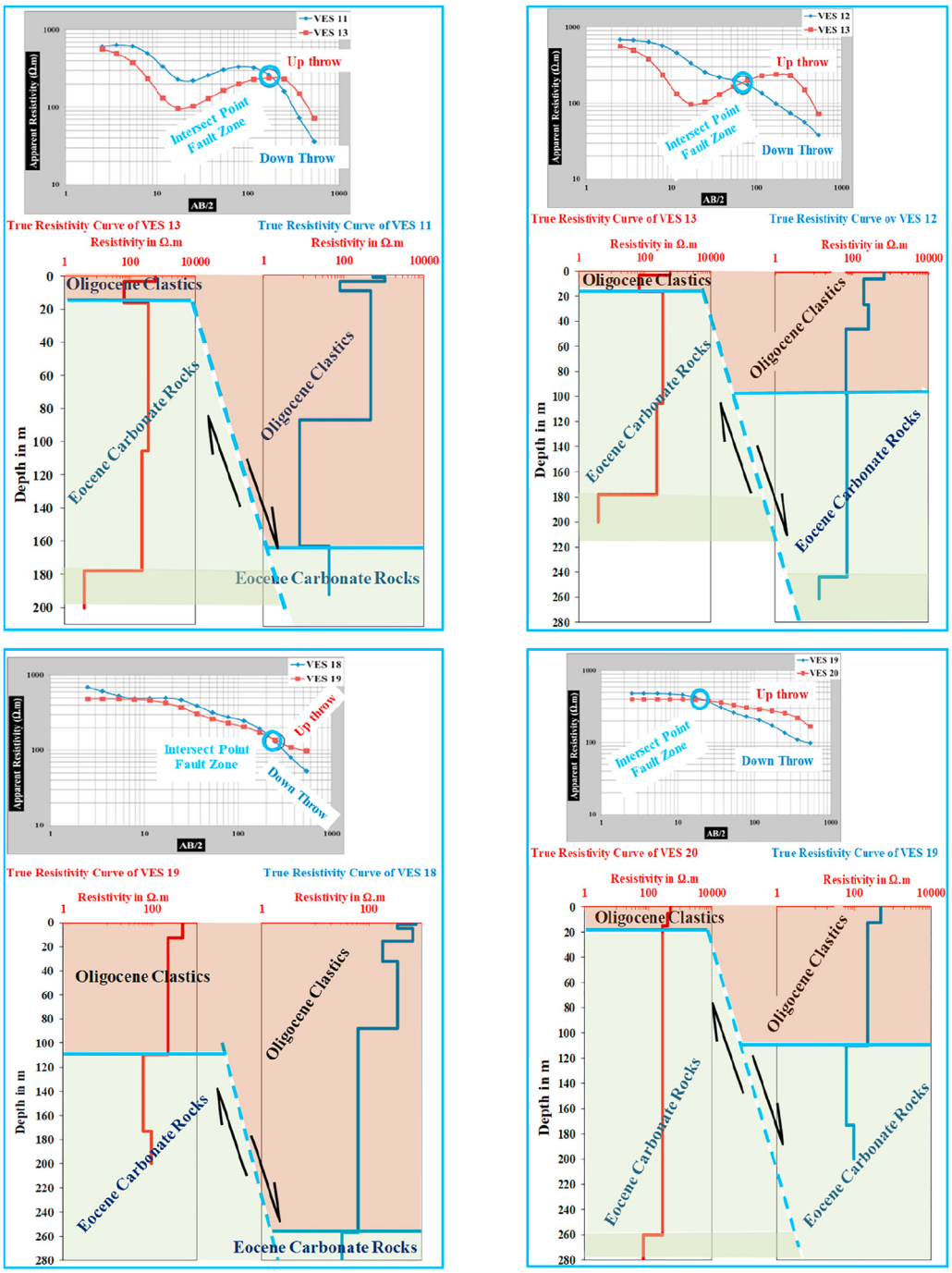

Figure 17. Four examples for delineating the expected fault zone between the different VESs along the sections are between the VES11 and VES13 (upper left), (the VES12 and VES13 (upper right), (the VES18 and VES19 (lower left) and also, between the VES19 and VES20 (lower right))) from the intersection between their calculated resistivity curves according to the new assumptions by Ammar and Kamal (2018).

Oligocene Clastics aquifer, includes Gamma-ray log, single point resistance log, self-potential log, and short and long resistivity log, (Figure 18, right). These wells were analysed by using *Tech-log software*. Where *Didger software* was used for digitizing logs from image to get the Las file, which inputted to the Tech-log Las file. This file was included Gamma ray log and resistivity logs and caliber log. Accordingly, the Gamma ray log was used to indicate the amount of shale by using the formula 3. While the long-resistivity log was used to determine the porosity by using the two formulas 4 and 5, and Eq. (6).

The Gamma-ray was used to separate the shale or clay and shaly to pure sediments and calculate the volume of shale. While the long resistivity log was used to separate the highly shaly to pure saturated zones and calculate the porosity of these zones for the two aquifers as well, as assisting the other logs. The volume of shale was calculated by using the following formula:-

$$V_{sh} = \frac{(G_{log} - G_{max})}{(G_{max} - G_{max})} \quad (3)$$

(Schlumberger, 1972)

While the porosity was calculated by using the following formulas:-

$$F = \frac{\rho_t}{\rho_w} \quad (4)$$

(Archie's formula, 1942)

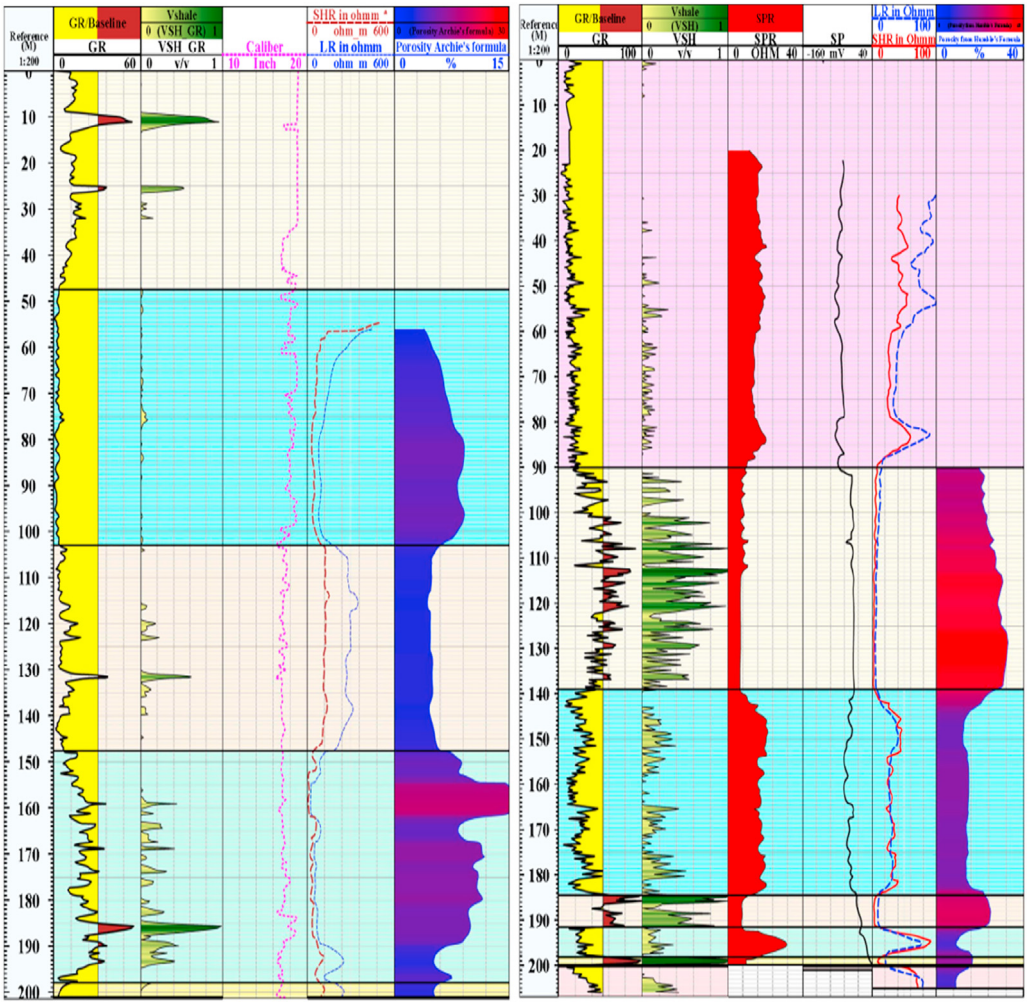

Figure 18. Geophysical well logging data and their analysis for well (1) at the Eocene Carbonate aquifer (left), that includes from left to right: the Gamma-ray log, volume of shale, calibre log, short and long resistivities logs, and porosity values. While well (5) at the Oligocene Clastics aquifer (right) includes from left to right: the Gamma-ray log, volume of shale, single point resistance log, Self-Potential log, short and long resistivities logs, and porosity values.

$$F = 0.62/\Phi^{2.15} \quad (5)$$

(Humble's formula)Where: ρ_t is the true resistivity of the formation from long-resistivity log, ρ_w is the water resistivity, and Φ is the porosity in percentage %. The ρ_w was calculated from the following equation:-

$$\rho_w = \frac{640}{\text{T.D.S}} \quad (6)$$

The Archie's formula was used to determine the porosity of the limestone aquifer, as shown in well (1) (Figure 18, left), while the Humble's formula was used to calculate the porosity in the Oligocene Clastics, as shown in well (5) (Figure 18, right). The measured values of the total dissolved solids (T.D.S) in well (1) was 966 ppm and in well (5) was 910 ppm were used for calculating the resistivity of water.

Also, the deep (long) resistivity and Gamma-ray logs were correlated with the measured soundings and found that, there is good matching with the soundings outputs in the carbonate aquifer like TEM2, then have good matching with the soundings outputs in the Oligocene Clastics like VES9 and TEM12. Accordingly, from the analysis of well logs, the volume of shale was ranged from 0% to 100% at the limestone and Oligocene aquifers. These ranges reflect that, the estimated high to low resistivity values of the recorded layers from the VESs and TEMs are due to the decrease to increase the shale volume, respectively, like limestone to shaly limestone and shale and clayey Oligocene Clastics to clay. Also, the estimated high to low resistivity values of these layers are affected by the porosity values which are ranged in the Oligocene aquifer from ~9% to ~35%, while in the limestone aquifer ranges from ~4% to ~15.5%, as reported in Figure 18.

4. Summary, conclusion, and recommendations

For this study, the DC-resistivity method (VESs) and Transient Electromagnetic method (TEMs) were used for manifesting the electrical, geological and hydrogeological characteristics of the aquifers using the forward and inverse modeling. The selected area for carrying and applying this study was West El-Minia city. *Geologically*; this area consists mainly of Samalut Formation, made up of limestone with shale intercalation, underlined by El-Minia Formation that, consist of limestone, as well as Oligocene Clastics that, made up of sand, gravel, with clay intercalation. *Structurally*; this area was subjected to intense uplifting, as shown from the ground elevations and topographical features in which the main structure features are the faults. *Hydro-geologically*; there are three main aquifers, these are the Oligocene clastic aquifer, the Carbonate aquifer, and the Nubian Sandstone aquifer. This study focuses on exploring, studying and delineating the characteristics of the Oligocene Clastics and Eocene Carbonate aquifers. The Eocene Carbonate aquifer is considered the main shallow and deep aquifer and more extended than the Oligocene Clastics aquifer.

Accordingly, 22 VESs, using Schlumberger configuration (AB/2 = ~500–~700m), were carried out for studying the shallow resistive section, detecting the shallow Oligocene aquifer and the shallow depths of the Eocene aquifer, as well as delineating the dissecting faults. Also, 12 TEMS were carried out, using the in-loop configuration (square ℓ = 200m) for studying and detecting the shallow and deep conductive layers. The characteristics of aquifers were estimated, using the forward (initial) model and the inverse (layered) model for interpreting the VESs data, using Zohdy and Bisdorf technique (1989) and Rinvert software (1999), and the TEMs data, using *Steminv and Tcinv softwares*. This interpretation was controlled by the accuracy in data measurements and the available shallow and deep hydrogeological data from the drilled wells and well logging data.

The inverse models of the VESs and TEMs were calibrated and translated the subsurface electrically, geologically and hydrogeologically into four units; dry Oligocene Clastics (173–467 Ω.m), dry limestone (273–374 Ω.m), saturated Oligocene Clastics (Oligocene aquifer) (2 Ω.m, due to the increase in clay content and salinity values (~900–~6800 ppm) -107 Ω.m), then the saturated fractured limestone to shaly limestone (Eocene carbonate aquifer) (5 Ω.m, due to the increase in shale content, salinity values and also in the fracture density with the high in salinity, -188 Ω.m). Also, these inversion models assisted in estimating the depths to groundwater (62m–131m) and in choosing the promising locations for drilling productive wells.

Accordingly, two hydro-geo-electrical sections were built for simulating the resistivity values of the resistive and conductive layers, vertically and horizontally, and showing the resolution of the shallow and deep sections, as well as their thickness variations. The resistivity values indicated that, the shale content at the limestone layers increases toward the north-western parts and the thickness of the Oligocene Clastics increases toward the south and southwest and it disappears toward the north. Also, it is found that, the area was subjected to several faults affected on the geological and hydrogeological implications.

The ramp-off time effect was studied for the measured TEMs data and found that, due to the primary and secondary magnetic fields interference in the early time of receiving the TEM response and the high resistivity small thickness effect, ~50m–~100m of shallow depths didn't recorded as matched with the VESs analysis, the max penetration depth of TEMs was 672m. There are varying recorded logs include Gamma-ray, short and long resistivity, and calibre logs for the Eocene Carbonate aquifer, and also include Gamma-ray, single point resistance, Self-Potential and short and long resistivity logs for the Oligocene Clastics aquifer. These logs were analyzed, using the *Techlog software*, that revealed the pure and shale saturated zones, the volume of shale is ranged between ~0% and 100% at the two aquifers, and the porosity in Oligocene aquifer is varied from ~9% to 35% while in the carbonate aquifer it attains ~4%–15.5%. These values are controlled by the hydrogeological conditions, as estimated and matched with the inverse model outputs of the geo-electrical soundings.

At the end, it can be concluded that, the understanding of the forward and inverse models for the VESs and TEMs interpretation and the integration between these soundings are considered as efficient way for solving several problems during their interpretation and for increasing the accuracy in estimating the complicated geological and hydro-geo-electrical characteristics of the aquifers. Also, it should use a low ramp transmitter for identifying the high resistive shallow depths, especially at the high resistive areas like the area under study for reducing the ramp-off time effect.

Declarations

Author contribution statement

A. I. Ammar, A. A. Mustafa: Conceived and designed the experiments; Performed the experiments; Analyzed and interpreted the data; Contributed reagents, materials, analysis tools or data; Wrote the paper.

A. S. A. Abu El-Ata: Conceived and designed the experiments; Contributed reagents, materials, analysis tools or data; Wrote the paper.

A. M. S. Lala: Conceived and designed the experiments.

Funding statement

This research did not receive any specific grant from funding agencies in the public, commercial, or not-for-profit sectors.

Data availability statement

The authors are unable or have chosen not to specify which data has been used.

Declaration of interests statement

The authors declare no conflict of interest.

Additional information

No additional information is available for this paper.

Acknowledgements

Thanks are due Research Institute for groundwater (RIGW), National Water Research Center, for helping to carry out the field measurements and collect the field data including hydrogeological and geological maps. We would like to thank the hydrogeological professors at the institute and the reviewers for comments and editing that helped in manuscript improvement. Also, we special thankful for the Editor-in Chief and Co-Editor-in-Chief for interesting and assisting in publishing this article.

References

Albouy, Y., Andrieux, P., Rakotondrasoa, G., Ritz, M., Descloitres, M., Join, J.L., Rasolomanana, E., 2001. Mapping coastal aquifers by joint inversion of DC and TEM soundings—three case histories. Ground Water 39 (1), 87–97.

Ammar, A.I., Kamal, K.A., 2018. Resistivity method contribution in determining of fault zone and hydro-geophysical characteristics of carbonate aquifer, eastern desert, Egypt. Appl. Water-Sci. 8 (1), 1–27.

Archie, G.E., 1942. The electrical resistivity log as an aid in determining some reservoir characteristic. Trans., AIME l, 146.

Carrasquila, A.A.G., Ulugergerli, E., 2006. Evaluation of the transient electromagnetic geophysical method for stratigraphic mapping and hydrogeological delineation in campus basin, Brazil. Rev. Bras. Geofís. 24, 333–341.

Christensen, N.B., Sørensen, K.I., 1995. New Strategies for Surface and borehole electric and electromagnetic methods for hydrogeophysical investigations. Eur. J. Environ. Eng. Geophys. 3, 75–90.

Danielsen, J.E., Auken, E., Jorgensen, F., Sondergaard, V., Sørensen, K.I., 2003. The application of the transient electromagnetic method in hydrogeophysical surveys. J. Appl. Geophys. 53 (4), 181–198.

El sayed, A.N., 2016. The impact of geologic setting on the groundwater occurrence in the Eocene limestone of El Minia-East Nile-Egypt, using geoelectrical technique, Pelagia Research Library. Adv. Appl. Sci. Res. 7 (4), 257–273.

Fitterman, D.V., Anderson, W.L., 1987. Effect of transmitter turn-off time on transient soundings, Netherlands. Geoexploration 24, 131–146.

Fitterman, D.V., Stewart, M.T., 1986. Transient electromagnetic sounding for groundwater. Geophysics 51, 995–1005.

Flathe, H., 1955. Possibilities and Limitations in Applying Geoelectrical Methods to Hydrogeological Problems in the Coastal Areas of North West, 3. Geophys Prospect, Germany, pp. 95–110.

Flores, C., Romo, J.M., Vega, M., 2013. On the estimation of the maximum depth of transient electromagnetic soundings: the case of the Vizcaino transect, Mexico. Geofisc. Int. 52 (2), 159–172.
Goldman, M., Neubauer, F., 1994. Groundwater exploration using integrated geophysical techniques. Surv. Geophys. 15, 331–361.
Goldman, M., Plooy, A.D., Eckard, M., 1994. On reducing ambiguity in the interpretation of transient electromagnetic sounding data. Geophys. Prospect. 42, 3–25.
Hantar, G., 1990. North Western Desert. In: Said, R. (Ed.), The Geology of Egypt. Balkema, pp. 293–319 chapter 15.
Issawi, B., El Hinnawi, M., Francis, M., Mazhar, A., 1999. The Phanerozoic geology of Egypt A Geodynamic Approach. special publication, Cairo, p. 462 no. 76.
Jens, E.D., Auken, E., Jørgensen, F., Søndergaard, V., Sørensen, K.I., 2003. The application of the transient electromagnetic method in hydrogeophysical surveys. J. Appl. Geophys. 53, 181–198.
Jorgensen, F., Sandersen, P.B.E., Auken, E., 2003. Imaging buried Quaternary valleys using transient electromagnetic method. J. Appl. Geophys. 53, 199–213.
Khalifa, M.A., 1981. Geological and Sedimentological Studies of West BeniMazar Area, South El-Fayum Province, Western Desert, Egypt. Ph.D. Thesis.
Khalil, M.A., Abbas, A.M., Santos, F., Massoud, U., Salah, H., 2013. Application of VES and TDEM techniques to investigate seawater intrusion in Sidi Abdel Rahman area, northwestern coast of Egypt. Arab. J. Geosci. 6, 3093–3101.
Klitszch, E., List, F.K., Pohlmann, G., 1987. Geological Map of Egypt. Conoco Coral and Egyptian General Petroleum Company, Cairo, Egypt. 24 Sheets, Scale 1:500 000, NH 36 SW Beni Suef.
Kruse, S.E., Brudzinski, M.R., Geib, T.L., 1998. Use of electrical and electromagnetic techniques to map seawater intrusion near the Cross-Florida Barge Canal. Environ. Eng. Geosci. 4, 331–340.
Massoud, U., El Qady, G., Metwaly, M., Santos, F., 2009. Delineation of shallow subsurface structure by azimuthal resistivity sounding and joint inversion of VES–TEM data: case study near Lake Qaroun, El Fayoum, Egypt. Pure Appl. Geophys. 166, 701–719.
McNeill, J.D., 1990. Use of electromagnetic methods for groundwater studies. In: Ward, S.H. (Ed.), Geotechnical and Environmental Geophysics, 1. Society of Exploration Geophysicists, Tulsa, Oklahoma, USA, pp. 191–218. Review and Tutorial.
Nabighian, M., Macnae, J., 1991. Time domain electromagnetic prospecting method in Chapter 6. In: Nabighian, M. (Ed.), Electromagnetic Methods in Applied Geophysics. Society of Exploration Geophysicists, Tulsa, pp. 427–520.
Norton, P., 1967. Rock – Stratigraphic Nomenclatures of the Western Desert, Egypt. Egypt Petrol. Corp.
Reynolds, J.M., 2011. An Introduction to Applied and Environmental Geophysics, second ed. Wiley-Blackwell, UK, p. 712.
RIGW, 1990. Hydrogeological Map of Egypt Report, Scale 1:100,000, first ed.
RIGW, 2015. Hydrogeological Map of Egypt, Five edition.
Rinvert, 1999. Geophysical Software Package: Licensed to Hydrogeology and Engineering Geology. Reg., Number, RW 140032, February 03, 1999, Hochi Minh City-Vietnam.
Said, R., 1962. The Geology of Egypt. Elsevier publication, co., Amsterdam, New york, p. 377.
Said, R., 1981. The Geological Evaluation of the River Nile. Springer-Verlag, New York, p. 151.
Schlumberger, 1972. Log Interpretation Volume 1–Principles.
Shata, A.,A., 1953. New light on the structural developments of the Western Desert of Egypt. Bull, Desert inst 1, 101–106.
Spies, B.R., 1989. Depth of investigation in electromagnetic sounding methods. Geophysics 54, 872–888.
Stewart, m., Gay, M.C., 1986. Evaluation of transient electromagnetic soundings for deep detection of conductive fluids. Ground Water 24 (3), 351–356.
Yousif, M., Sabet, H.S., Ghoubachi, Aziz A., 2018. Utilizing the geological data and remote sensing applications for investigation of groundwater occurrences, West El Minia, Western Desert of Egypt. NRIAG J. Aston. Geophys. 7 (2), 318–333.
Zohdy, A.A.R., 1969. The use of Schlumberger and equatorial soundings in groundwater investigations near El Paso. Geophysics, Texas 34, 713–728.
Zohdy, A.R., Bisdorf, R.J., 1989. Schlumberger Sounding Data Processing and Interpretation Program. U.S., Geological Survey, Denver, Co.